Observation of Terahertz Stimulated Emission of Radiation from Optically Pumped Graphene

Silvia H. Chan[1,2], Stephane Boubanga-Tombet[2], Amine El Moutaouakil[2], Akira Satou[2], and Taiichi Otsuji[2]

[1]*NanoJapan Program, Rice University and Department of Materials Science & Engineering, University of Pennsylvania*

[2]*Research Institute of Electrical Communication, Tohoku University, Sendai, Japan*

What's Graphene?

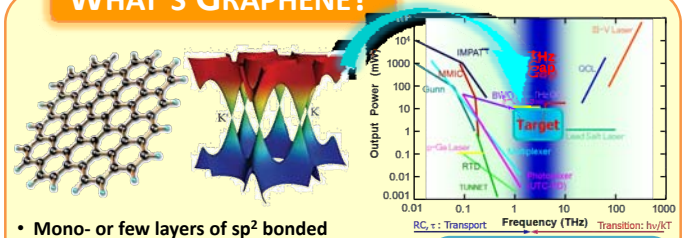

- Mono- or few layers of sp^2 bonded carbon atoms in a honeycomb lattice.
- Massless Dirac Fermions obey linear dispersion relation at K & K' points.
- High carrier mobility of 2 x $10^5 cm^2/Vs$ at RT. [1]

Due to its unique transport properties, graphene is suitable for implementation in photonic devices.

Objective

To stimulate terahertz (THz) emission by implementing electro-optic sampling (EOS) time-resolved spectroscopy to optically pump and THz probe exfoliated graphene ribbons (GR) on SiO_2 sample.

Theory

Non-equilibrium Carrier Dynamics in Optically Pumped Graphene[2]

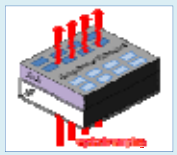

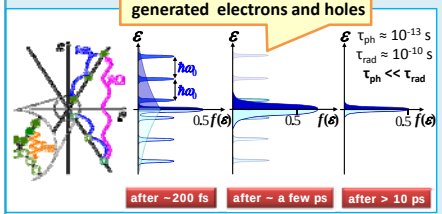

Optical pumping: $\hbar\Omega$
Optical phonon emission: $\hbar\omega_o$, τ_{ph}
Radiative recombination: $\hbar\omega$, τ_{rad}
=> THz emission

Non-equilibrium Negative Dynamic Conductivity

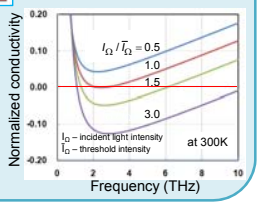

Electrons and holes relax and accumulate near the Dirac point. Due to graphene's negative dynamic conductivity in THz range, population inversion can be achieved for stimulated emission of THz lasing.

Setup & Method

1 Setup Laser Pathway for Pumping and Probing

Pump & Probe Pulses: 1.5μm, 80fs, 2mW

Bandwidth: ~7THz

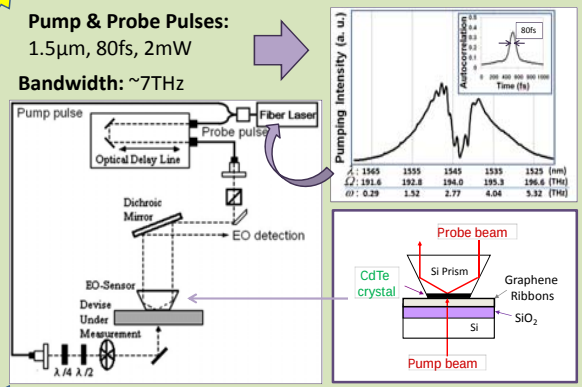

2 Excite Graphene with Femtosecond Pulse Laser

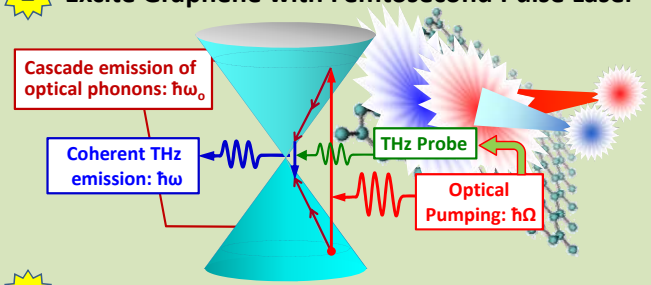

3 Isolate Graphene Response Peak & FFT to Obtain THz Emission Information

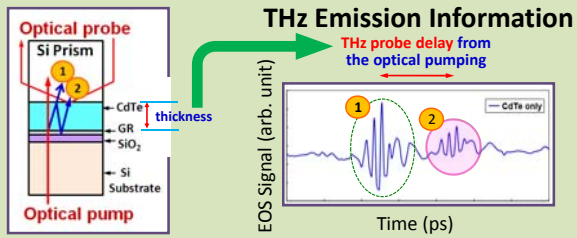

Results

1 Verification of THz Emission from Graphene

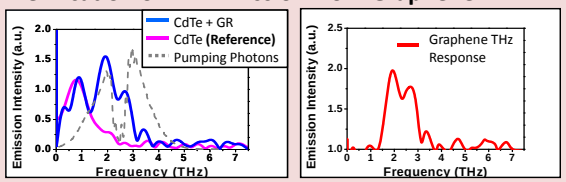

2 THz Emission Dependence on CdTe Crystal Thickness

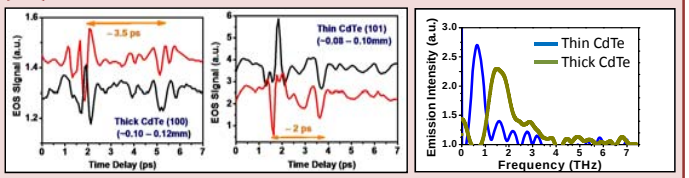

3 THz Emission from Monolayer vs. Bilayer GR

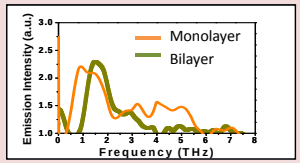

Conclusions

- **THz coherent emission was successfully observed** in optically pumped graphene.
- **Thinner CdTe gives rise to an emission spectra shifted to lower frequencies compared to those of the thicker CdTe**. This discrepancy might be attributed to the usage of a different crystal orientation.
- **The emission spectra of monolayer GR was found to be broader than those of bilayer GR**. The parabolic band structure of bilayer GR accelerate relaxation dynamics and gives rise to narrow spectra at lower frequencies.

Future Work

- Use the (100) crystal orientation CdTe of varying thicknesses to see the effects on the THz spectrum.
- Excite plain exfoliated graphene to verify the effect of plasmonic absorption of THz in GR sample.

Acknowledgements

Research conducted at Otsuji Laboratory of Tohoku University as a participant of the NanoJapan 2010 program, sponsored by Rice University and the NSF-PIRE Grant. http://nanojapan.rice.edu

References

1. S.V. Morozov et al. PRB 100, 016602 (2008)
2. V. Ryzhii, M. Ryzhii, T. Otsuji, J. Appl. Phys. 101, 083114 (2007)

This material is based upon work supported by the National Science Foundation under Grant No. OISE-0530220.

The Study of Tip-Induced Deformations in Single-Walled Carbon Nanotubes Using Tip-Enhanced Near-Field Raman Spectroscopy

Warren Cheng[1,2], Shota Kuwahara[2], and Satoshi Kawata[2]

1.NanoJapan Program, Rice University and Columbia Laboratory for Unconventional Electronics, Department of Electrical Engineering, Columbia University, NYC, USA

2. Laboratory for Scientific Instrumentation and Engineering, Department of Applied Physics, Osaka University, Osaka, Japan

Background

Raman Spectroscopy

Fig. 1 – Raman Spectroscopy

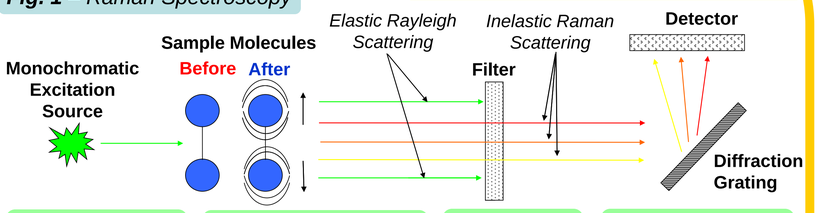

1. Mono. Source Excites Sample → 2. Molecules Vibrate & Scatters Light → 3. Rayleigh Removed → 4. Raman Spectra Detected

Carbon Nanotubes (CNT)

- Possess electronic and vibrational properties which are dependent on the CNTs' chirality (detected with Raman spectroscopy)

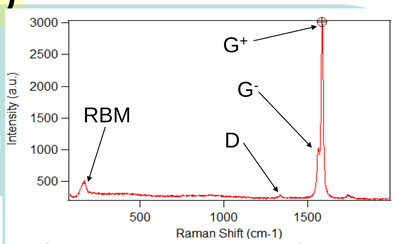

Fig. 2 – Raman Spectrum of CNT

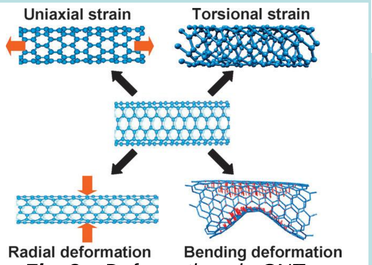

Fig. 3 – Deformations in CNT
Z. Liu, et. al., Chem. Comm.2009, 6902 (2009).

- Deformations alter the CNTs' energy band structure thereby altering their characteristics
- Shifts in the phonon modes result from these alterations

Significance

- **Far-field Raman Spectroscopy** has **low spatial resolution ~300nm** – (*due to diffraction limit of propagating light* ***d = λ/2***)
  Tip-Enhanced Raman Spectroscopy (TERS) can achieve a spatial resolution of less than 30nm
- **Raman Scattering** is **very weak** compared to **Rayleigh Sct.** (**~1 in 10 million photons** in a scattering event are Raman!)
- **Manipulation of CNTs** could cause **loss in Raman intensity**
  TERS increases the Raman Scattering response by a factor of 10^0 - 10^4

Method

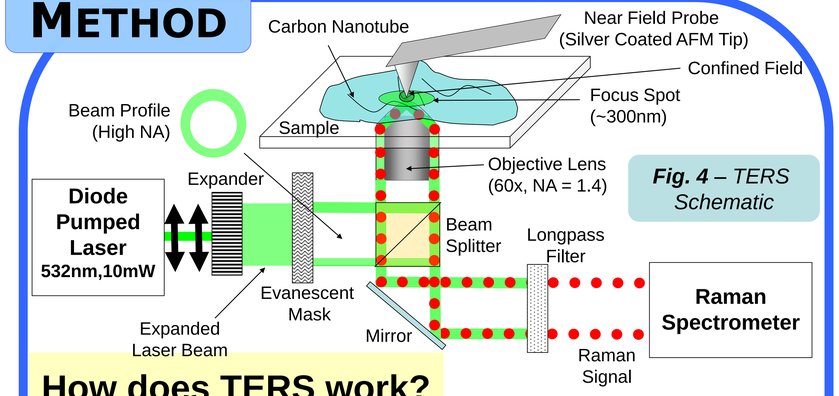

Fig. 4 – TERS Schematic

How does TERS work?

- ***Evanescent illumination*** decreases the spot size of the laser confining the illuminated region of the sample
- **High NA p-polarized component** of the laser increases the electromagnetic field along the metallized tip
- Propagating photons are captured and confined at the apex of the hovering conical ***silver coated silicon tip*** due to coupling with localized ***surface plasmon polaritons***

Process

1 Spincoated and then baked **CoMoCAT SWCNT** onto glass slides

2
- Used an **AFM-Raman System** comprised of a SII AFM system and Nikon Optical Microscope
- **Far-field image** of the SWCNT was taken by raster scanning the sample with the setup in Fig. 4 but ***with the tip and evanescent mask removed***

3 Using a silicon **Dynamic Force Microscopy (DFM)** tip, a ***~430 nm horizontal defect*** was introduced

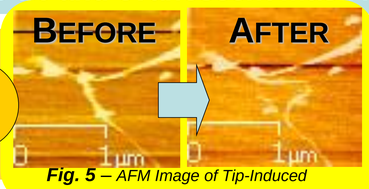

Fig. 5 – AFM Image of Tip-Induced Deformation in CNT

4 **Far-field** (as in step 2) and **near-field** (using the setup of Fig. 4 with the tip constantly over the focal point) images of the manipulated SWCNT were taken

Results

Manipulation region was about 5 nm wide - determined with DFM
Indicates a bundled structure containing 4 or 5 SWCNT

1 Before Manipulation — **Far-field**

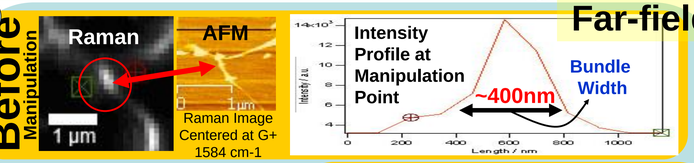

2 After Manipulation

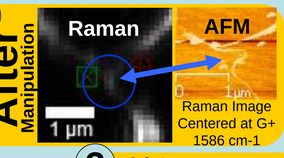

Raman Spectra At Manipulation Point

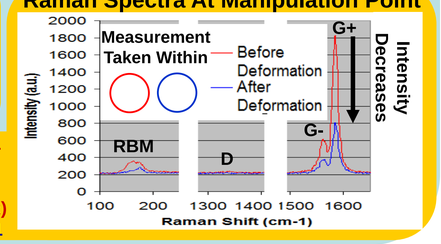

3 Peak Shift
- ΔG+ = 1.7 cm-1
- ΔG- = 1.3 cm-1
- ΔD = N/A (Low SNR)
- ΔRBM = 8 cm-1

Near-field

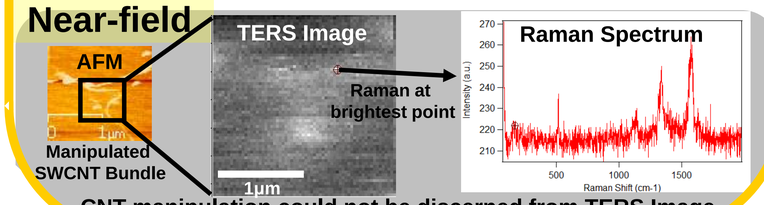

CNT manipulation could not be discerned from TERS Image

Conclusion

- **TERS** was *not supported* by results, but it still exists
- **Proved** the ***necessity of TERS*** because:
  1. **~5nm** bundle was measured **~400nm** using Far-field
  2. D-band was **indiscernible from noise** after defect
- **RBM peak shift** could indicate a shift in the orientation of the bundled CNTs or change in CNT band structure

Future Work

- Work with a single CNT strand instead of bundle
- Obtain data showcasing TERS enhancement
- Develop new opto-electric devices using the SWCNT structural deformation relation to electronic structure

This material is based upon work supported by the National Science Foundation under Grant No. OISE-0530220.

http://nanojapan.rice.edu

Acknowledgements

I would like to sincerely thank Prof. J. Kono, Dr. C. Matherly, K. Packard, S. Phillips, and Prof. C. Stanton of NanoJapan 2010 for developing such an amazing program that enabled me to achieve this dream. Thanks to Prof. S. Kawata for giving me the opportunity to work at LaSIE, to Y. Okuno for his helpful lessons, to the members of LaSIE and to last but certainly not least Dr. S. Kuwahara for his endless patience and guidance for without whom I could not have accomplished such a project.

Chemical Vapor Deposition Synthesis of Graphene from Alcohol

Kevin Chu[1,2], Bo Hou[2], Xiao Chen[2], Pei Zhao[2], Erik Einarsson[2], Shohei Chiashi[2] and Shigeo Maruyama[2]

[1]*NanoJapan Program and Department of Electrical & Computer Engineering, Rice University*

[2]*Department of Mechanical Engineering, The University of Tokyo*

Introduction

➢ **Graphene** is a 2D sheet of sp^2-hybridized carbon.

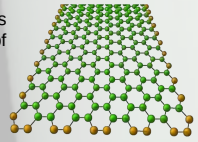

Right: Graphene molecular structure

➢ Graphene synthesis methods: Mechanical exfoliation, oxidation of graphite, liquid-phase exfoliation and epitaxial growth such as chemical vapor deposition (CVD).

Above: Graphene field-effect transistors

➢ Why CVD? Higher quality Larger quantity

Above: SEM image of crumpled graphene

➢ Why Alcohol? High purity carbon source.

➢ Potential applications include: Graphene transistors, ultracapacitors, solar cells and flexible displays.

S. Maruyama et al (2010). Y. Lin al., *NanoLett.* (2009). A. Geim et al., *Nano Lett.* (2005).

Experimental

➢ **CVD**

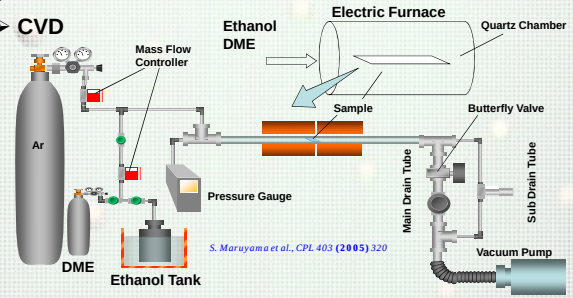

➢ **CVD Procedure**

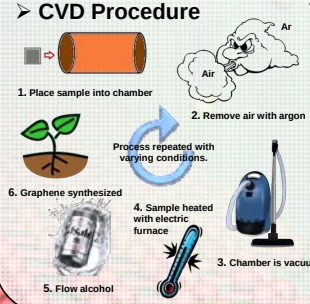

➢ **Raman**

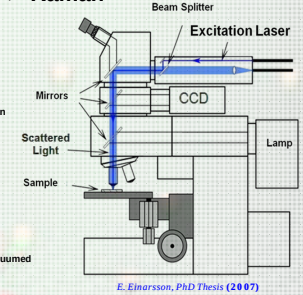

Results

➢ **CVD synthesis of graphene from EtOH on Ni foil**

Optimal Conditions:
EtOH(CH_3-CH_2-OH)
Temperature: 900°C
Pressure: 300 Pa
CVD Time: 5 Min

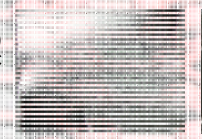

Below: Raman spectroscopy of the Ni Foil after having gone under CVD reaction.

Above: Photograph of the Nickel foil before undergoing CVD reaction.

Above: Photograph of Nickel foil after undergoing CVD reaction. Note the color changes. This sample is much darker.

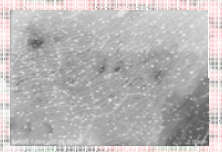

Above: SEM image of crumpled graphene on Ni substrate (x22.0k).

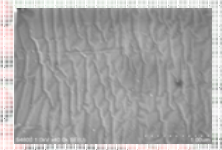

Below: SEM image of crumpled graphene on Ni substrate (x40.0k). **Graphene crumpled due to Ni expansion from high temperature.**

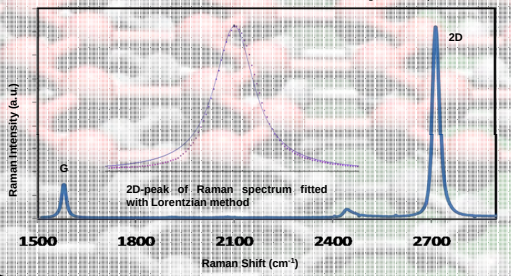

➢ **Discussion**

1. Graphene has a 2D & G peak ratio of 4.5 or greater.
2. Graphene's 2D-peak can be fitted with a single Lorentzian.
3. Both conditions were met as shown on the diagram to the left, we confirm the growth of graphene on Ni foil.

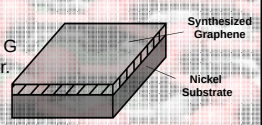

Results Cont'd

➢ **Surface Homogeneity**

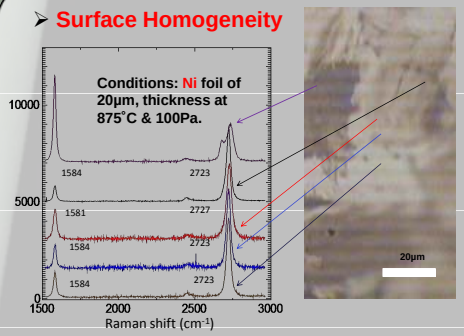

➢ **A Dilemma: Homogeneity & Quality**

1. We selected 5 points randomly on 5 samples of different temperatures and mapped out the relationship between 2D/G ratio and temperature.

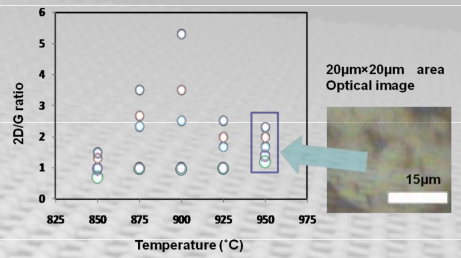

2. Quality graphene obtained at 875˚C and 900˚C.
3. Best surface homogeneity at 850˚C and 950˚C.
4. Difficult to synthesize both quality and homogeneous graphene.

➢ **CVD synthesis of graphene from Dimethyl Ether (DME) on Ni foil**

Purpose: To see whether DME can also synthesize graphene.

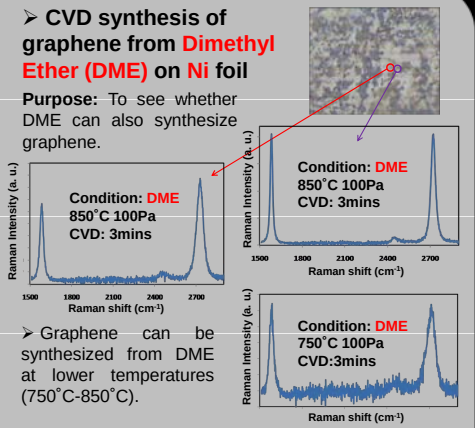

➢ Graphene can be synthesized from DME at lower temperatures (750˚C-850˚C).

➢ **CVD synthesis of graphene from EtOH on Cu foil**

Purpose: To see whether changing the substrate to Cu would allow us to produce graphene.

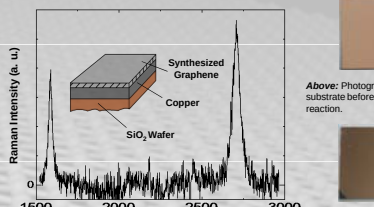

Above: Raman shift of copper sample after undergoing CVD. We confirm the growth of graphene on Copper.

Above: Photograph of the Copper substrate before undergoing CVD reaction.

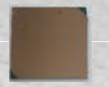

Above: Photograph of Copper substrate after undergoing CVD reaction. Note the color changes. This sample is much darker.

Conclusion

➢ We are capable of reproducing results of CVD synthesis of graphene on Nickel substrates with both ethanol and dimethyl ether as well as Copper substrates with ethanol.

➢ When using Nickel foil, high quality graphene can be obtained at 875˚C and 900˚C.

➢ When using Nickel foil, surface homogeneity is better achieved at 850˚C and 950˚C.

➢ Copper substrates can be used for graphene synthesis; however, surface homogeneity is difficult to achieve.

➢ Graphene can be synthesized from DME at lower temperatures than ethanol (750˚C-850˚C).

Acknowledgements

This material is based upon work sponsored by the NSF under Grant No. OISE-0530220.

We thank Dr. Junichiro Kono, Ms. Sarah Phillips, Dr. Keiko Packard and Dr. Cheryl Matherly for organizing NanoJapan 2010.

Poster Background, J. Warner et al., *Nature Nanotechnology, Vol 4.* (2009)

Fabrication and Characterization of Carbon Nanotube Field-Effect Transistors

M. Diasio,[1] H. Gojuki,[2], D. Kato,[2] T. Ohya,[2] A. Subagyo,[2] and K. Sueoka[2]

1. NanoJapan Program and Department of Physics and Astronomy, Rice University

2. Graduate School of Information Science and Technology, Hokkaido University, Sapporo, Japan

Background

Carbon Nanotubes (CNT)

- Semiconducting or metallic
- Weak spin-orbit coupling

CNT Field-Effect Transistors (CNTFETs)

- Possible spintronic applications
- Cannot control junction resistance due to varying CNT properties
- End contact geometry – efficient charge carrier transport?

Side contact

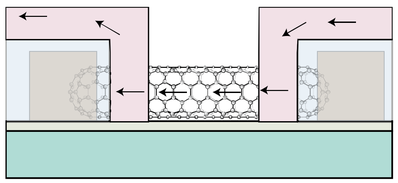

End contact

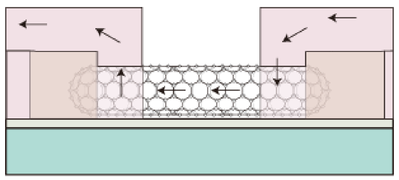

Purpose

- Realization of end contact junction between metal and CNT
- Fabrication of CNTFET with end contact junction
- Fabrication of CNT spin devices with end contact junctions

Methods

- Start with standard photolithography and chemical vapor deposition for CNT, with a HfO_2 top layer
- Changes for end-contact FET fabrication

Dry etching

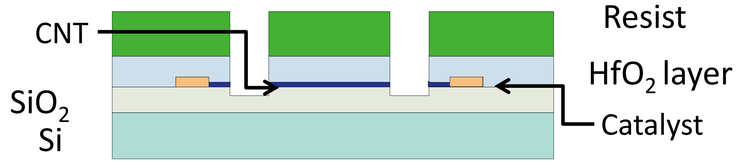

Lift off and recoat

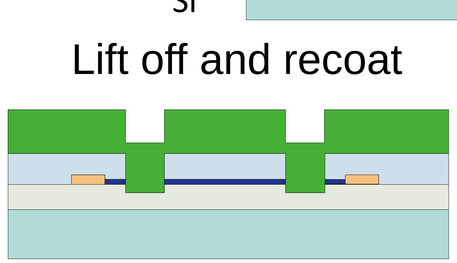

Electrode deposition

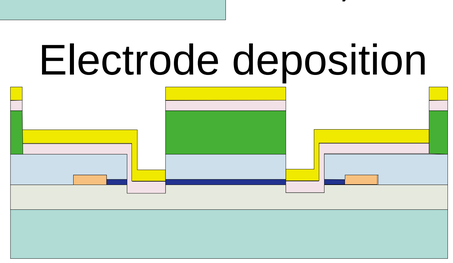

Completed CNTFET spin device

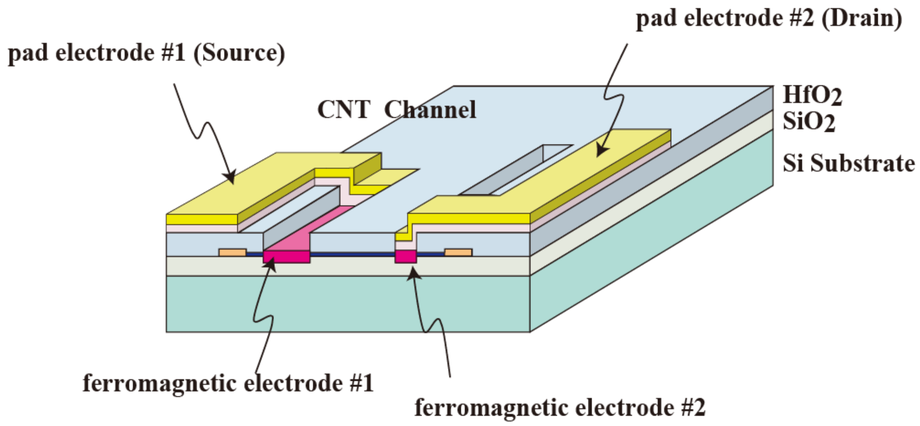

- Measure current-voltage response at different temperatures

Results

I_d-V_g of a CNTFET with a Pd electrode, T=290K

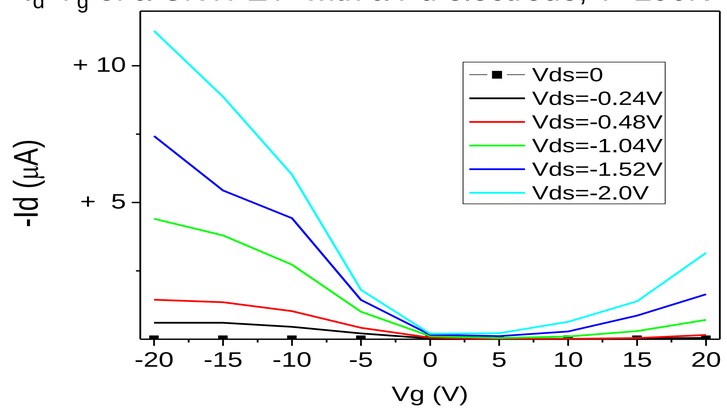

I_d-V_g Characteristics of CNTFETs with Ti electrodes

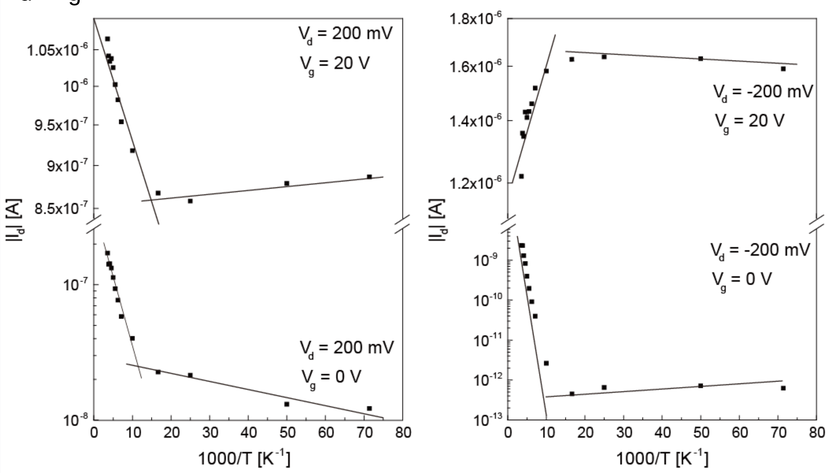

Side contact

End contact

Conclusions and Future Work

- Can fabricate CNT devices with end contacts
- Palladium shows controllable current response
- End contact does not form Schottky barrier easily
- Characterize CNT spin device transport
- Evaluate effect of material on spin transport

http://nanojapan.rice.edu

This material is based upon work supported by the National Science Foundation under Grant No. OISE-0530220.

Lateral Quantum Dot Charge Sensor in a Mesoscopic Electron Transport System

Heerad Farkhoor[1,2], Tatsuki Takakura[3], Michel Pioro-Ladriere[4], Akira Oiwa[3], Seigo Tarucha[3]

1. NanoJapan Program, Rice University
2. Department of Electrical Engineering and Computer Science, The University of California- Berkeley
3. Department of Applied Physics, The University of Tokyo
4. Departement de Physique, Universite de Sherbrooke, Quebec, Canada

Theory

Quantum dot: The transport mechanism

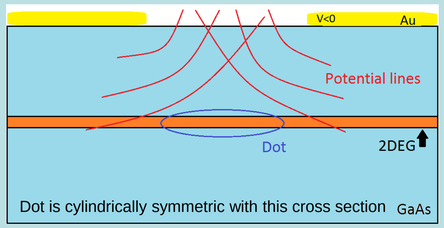

-Confinement of electrons in all three spatial directions

-Lateral dots confine a 2D electron "gas" layer electrically via metal surface gates

- Leads to discretized energy levels
  - Value and separation vary inversely on dot size
  - Controlled by varying voltage on a gate electrode
- Source and drain -> Single electron transistor

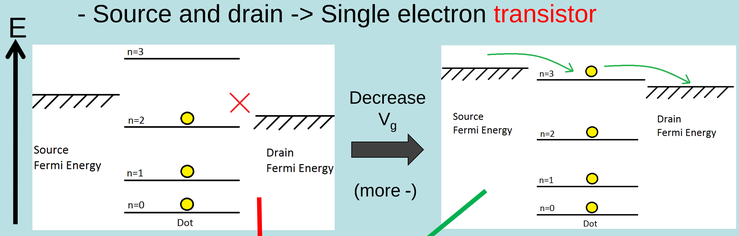

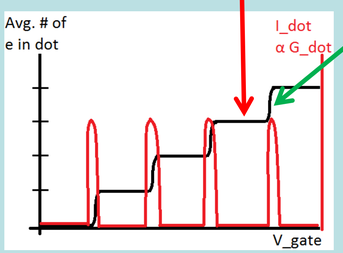

- Sweeping V_{gate} changes effective dot size -> shifts energy levels of dot

- Finite conductance when empty energy level is in window between S/D Fermi energies -> Coulomb oscillations

- Can place multiple dots in close proximity and analyze charge configurations
  - Electron vs. no electron, spin up vs. spin down
  - Charge state detection mechanism required
  - Quantum information processing applications

Quantum point contact: Traditional charge-sensing

- Narrow channel between two gates -> 2D of confinement

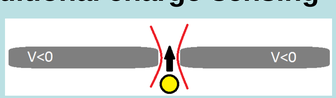

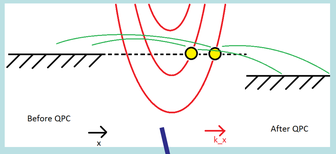

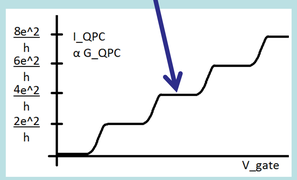

- Quantized conductance

- Parabolic shape from band structure, DC offset from gate-controlled confinement

- Each accessible "channel" adds 2e^2/h conductance

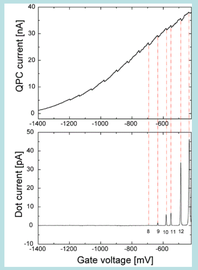

- **Nearby charges also affect the confinement in a QPC**
  - **Bias QPC at G transition point-> movement of charge will induce a noticeable change in the QPC current**
  - **Can be used as a charge-sensing signal**

Goal

- Improve charge sensor signal-to-noise ratio and sensitivity
  - Typical QPC: Sensitivity = 10%, SNR = 10

- QD more sensitive to potential fluctuations at transition point
  - Use a Sensor QD with I_{SQD} as the signal
  - 30 times more sensitive, 3 times better SNR than QPC

Design

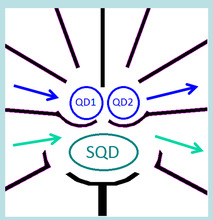

- Double quantum dot transport system

- Sensor quantum dot directly underneath

- Any two gates can be operated as a QPC

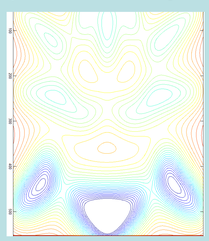

- Equipotential lines calculated for various gate positions and voltages

- Layout with strong coupling between dots, at least 200nm between gates, and ~ -1V operating point chosen for fabrication

Fabrication

1) MESA device and lead isolation structure patterned via UV photolithogrpahy

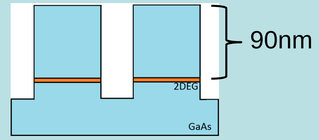

2) AuGe Ohmic substrate contacts patterned via UV photolithography, annealing drive-in

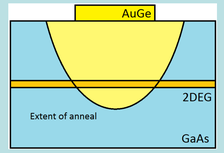

3) Ti/Au gate electrodes and leads patterned via EB lithography

4) Schottky gate contacts patterned via UV photolithography

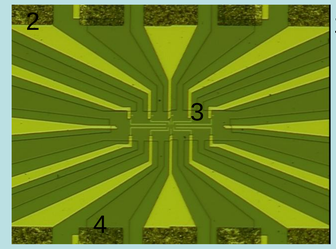

3

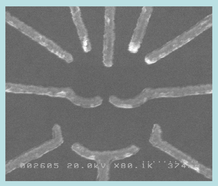

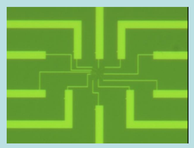

Results

-Unable to form dots that demonstrate Coulomb oscillation in 1.5K fridge due to shortage of time and a series of mishaps

Shubnikov-de Haas (2D)

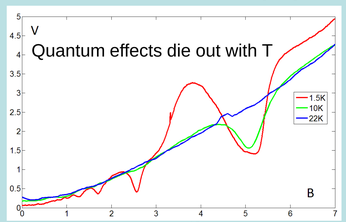

$$n = \frac{\nu e B(\nu)}{h} = \frac{1 \cdot 1.6\times10^{-19} \times 5.18}{6.63\times10^{-34}} = 1.25\times10^{15} e/m^2$$

QPC curve (1D)

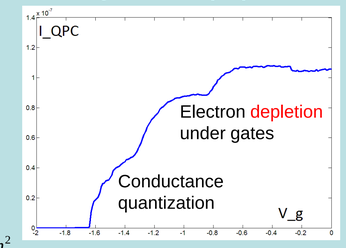

http://nanojapan.rice.edu

This material is based upon work supported by the National Science Foundation under Grant No. OISE-0530220.

Spin-dependent Tunneling Characteristics of Co2MnSi-based Magnetic Tunnel Junctions with $Co_{50}Fe_{50}$ Insertion Layers

Nabeem Hashem,[1,2] Tomoyuki Taira,[2] and Masafumi Yamamoto[2]

[1]NanoJapan Program, Rice University and Department of Physics, Yale University

[2]Division of Electronics and Informatics, Graduate School of Information Science and Technology, Hokkaido University, Sapporo, Japan

Introduction

Magnetoresistive Random Access Memory (MRAM)

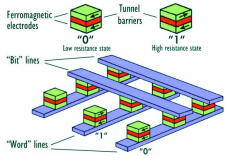

- Non-volatile
- High speed
- High density
- Unlimited read/write endurance
- **Principal switching component: magnetic tunnel junctions**

Magnetic Tunnel Junctions (MTJs)

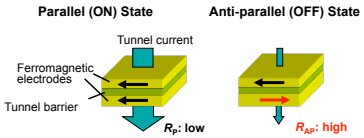

Key device parameter:

$$\text{TMR ratio} = \frac{R_{AP} - R_P}{R_P}$$

High spin-polarization is desirable to yield high TMR ratios

Heusler Alloy Half-Metallic Electrodes

- Complete spin polarization: only electrons of one spin involved in conduction
- Co_2MnSi (CMS) is a good candidate due to large energy gap for minority-spin electrons and high curie temperature

Purpose

- Previously demonstrated CMS/MgO/CMS MTJS with TMR ratios up to **236% at RT and 1135% at 4.2K** (Ishikawa et al., Appl. Phys. Lett. 2009)
- Large drop in TMR ratio at high T might be due to MgO/CMS in-gap interface states combined with magnon excitations

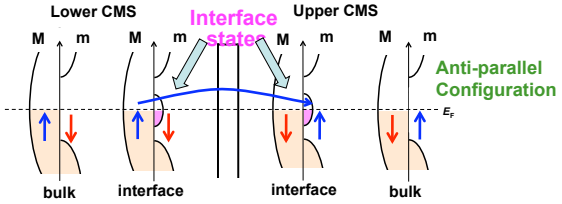

Purpose of this study is to understand this phenomenon in order to fabricate devices with higher TMR ratios

Methods

Approach

- Fabricate CMS-based MTJs with **interfacial insertion layers** in order to mitigate interfacial effects that tend to decrease TMR
- Measure and analyze the spin-dependent tunneling characteristics of these devices to elucidate tunneling paths

MTJ Fabrication

- MTJ layer structures were epitaxially grown on an MgO(001) substrate in a high vacuum chamber
- Layers deposited with magnetron sputtering and electron beam evaporation
- Samples processed using photolithography and argon ion milling

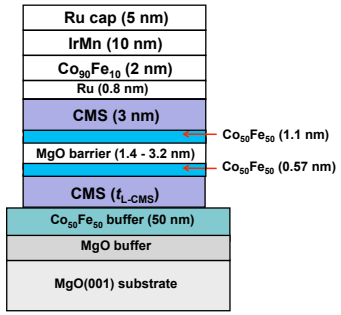

Results

TMR Characteristics

	TMR Ratio	
Layer structure	**RT**	**4.2 K**
MgO buff/CMS/MgO/CMS	**236%**	**1135%**
MgO buff/CoFe/MgO/CoFe	**250%**	**350%**
MgO buff/CoFe/MgO/CoFe/CMS	**450%**	**1135%**
MgO buff/CoFe buff/CMS/CoFe/MgO/CoFe/CMS	**413%**	**1523%**

- Presence of CMS dramatically improves TMR, indicating half-metallic characteristics
- Moreover, addition of insertion layers in CMS/MgO/CMS structures show further enhanced TMR

Acknowledgements: Research conducted at Hokkaido University as a participant in the Rice University NanoJapan 2010 program supported by the National Science Foundation under Grant No. OISE – 0530220. Special thanks to Prof. J. Kono, Prof. C. Matherly, and S. Phillips of the NanoJapan program for all their efforts.

Results (cont.)

Tunneling Spectroscopy

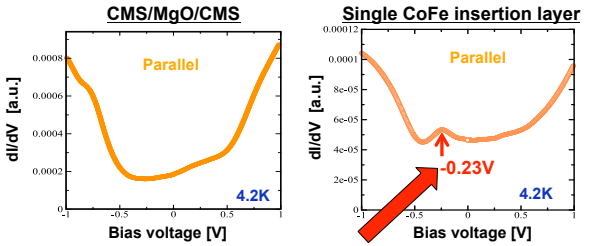

Peak at -0.23 V observed only in insertion layer MTJs

Discussion and Conclusion

Discussion

- Unique peak can be attributed to minority-to-minority tunneling path associated with the Δ5 symmetry (-0.22 eV to -0.30 eV)

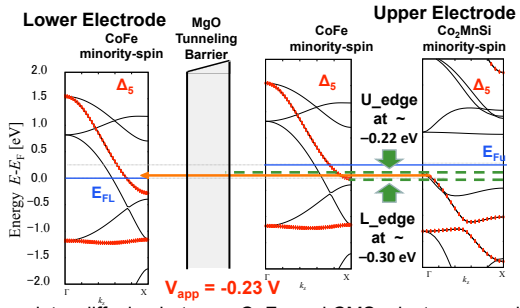

- Low inter-diffusion between CoFe and CMS: electrons supplied by CMS, and tunnel to lower electrode through CoFe
- Suggests that CoFe's primary role is to weaken magnon effects

Conclusion

- Demonstrated high TMR ratios up to 450% for CMS-based MTJs with $Co_{50}Fe_{50}$ insertion layers
- Tunneling spectroscopy confirmed that CMS acted as half-metallic spin-source while $Co_{50}Fe_{50}$ weakened magnon excitations
- **Future work:**
  - Understanding drop in TMR in double insertion layer MTJs
  - Further optimizing interfaces to enhance TMR

Fabrication of GaAs nanowires for solar cell devices

Y. Lai[1,2], E. Nakai[2], K. Hiruma[2], and T. Fukui[2]

1. *NanoJapan Program, Rice University and Department of Electrical & Computer Engineering, Massachusetts Institute of Technology*

2. *Research Center for Integrated Quantum Electronics, Hokkaido University, Sapporo, Japan*

Introduction

In this experiment, we will use selective-area metal-organic vapor-phase epitaxy (MOVPE) to fabricate planar and nanowire solar cells. We will further test the I-V Characteristics under Air Mass 1.5 Global (AM1.5G) standard illumination and the reflectances of the devices and compare their performances.

Advantages to periodically-aligned core-shell nanowire (NW) arrays for solar cells

- The nanowire is long in the direction of incident light, improving the light absorption; but then short in the other dimension, allowing for effective carrier collection.
- Shell structure of the nanowire increases the depletion region area, enhancing carrier collection.
- The nanowire structure reduces the reflection, and increases the absorption at high frequency.
- Nanowire solar cell requires less materials.

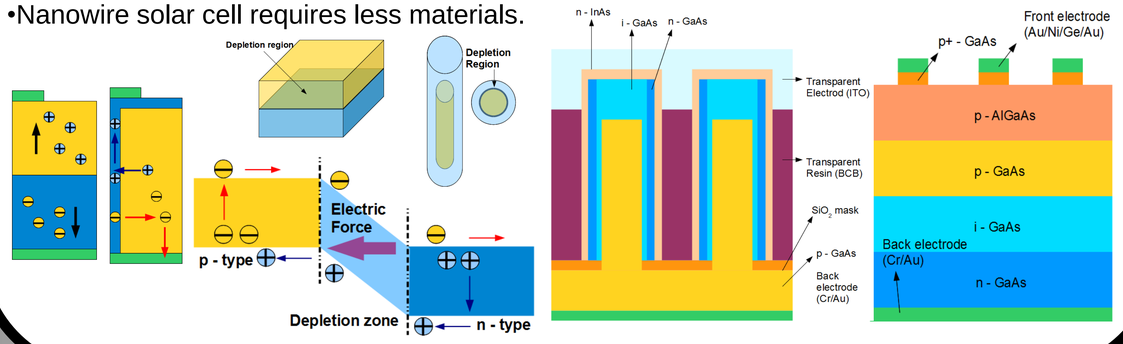

Methods

Mask Pattern Development

- Sputter SiO_2 on p-type GaAs(111)B substrate

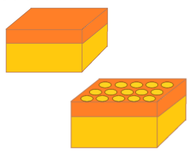

- Develop hexagonal lattice mask pattern using electron beam (EB) lithography and wet chemistry

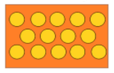

SA-MOVPE Growth

(1) T_G = 750°C (2) T_G = 750°C

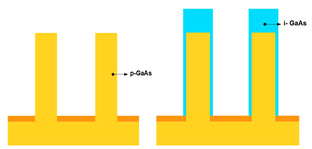

(3) T_G = 680°C (4)T_G = 680 °C

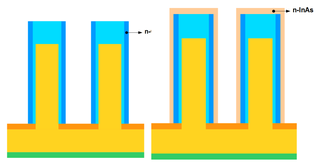

Device Fabrication

(1) Insulate NWs with resin (BCB) via spin-coating

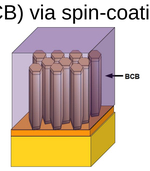

(2) Expose NW tips via reactive ion etching (RIE)

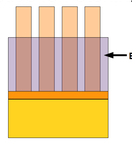

(3) Deposit transparent electrode (ITO) via sputtering

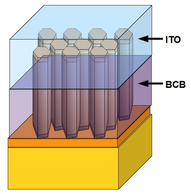

(4) Deposit the back electrode (Cr/Au) using Electron Beam Evaporation method

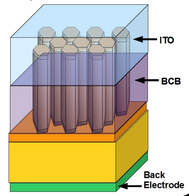

Results

SEM Images

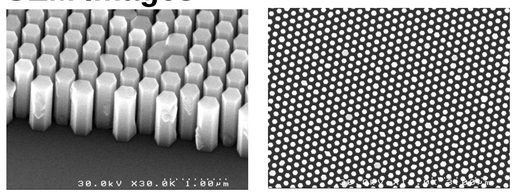

Core-shell Nanowires

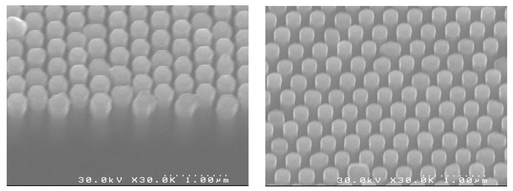

Nanowires with BCB

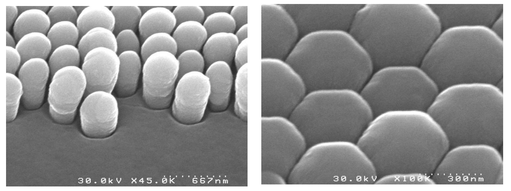

Nanowires with BCB and ITO

Grown NW Observations

Height = 1.1μm
Diameter = 80 nm
Pitch = 400 nm

I-V Characteristics of Nanowire Solar Cell

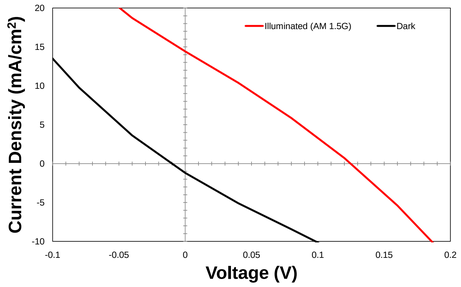

ISC = 14.4286 (mA/cm^2)
VOC = 0.124688 (V)
Imax = 7.806 (mA/cm^2)
Vmax = 0.064 (V)

FF = 0.27769
η = 0.49958%

The Reflectance of Nanowire and Planar Solar Cells

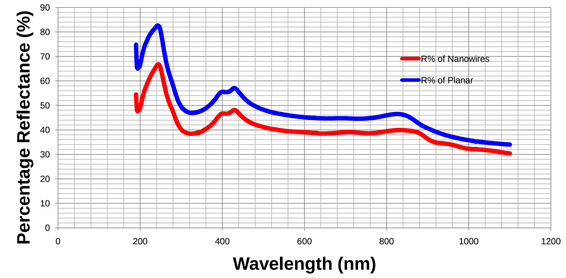

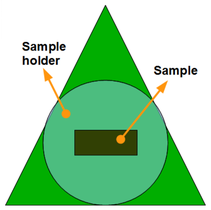

Machine Condition:

The diameter of the sample holder is 5mm, and the dimension of the sample is 3mm x 1mm. Due to the hole of the sample holder is bigger than the sample of NW solar cell, the reflectance of NW solar cell is lower than the reality. For example, according to the data, the reflectance of planar solar cell is 45% and the NW solar cell is 40%; while in the reality the reflectance of NW solar cell is 10~11%.

Conclusions and Future Works

- Successfully fabricate planar solar cell and core-shell nanowire solar cell using MOVPE and developed fabrication process for GaAs NW photovoltaic device
- In the future, the device can be optimized by adjusting geometrical parameters such as array pitch size and NW diameter/length, as well as NW growth conditions
- The quantum efficiency of solar cell can also be improved by adding buffer layers in the nanowires to more effectively separate the electrons

Acknowledgements

This material is based upon work supported by the National Science Foundation under Grant No. OISE-0530220. http://nanojapan.rice.edu

Structural Characterizations Of Thermally Treated DNA-Dispersed Double Walled Carbon Nanotubes

E. Landry,[1,2] K. Komiyama,[2] M. Hori, [2] J.S. Park,[2] Y.A. Kim,[2] and M. Endo[2]

[1]Department of Chemical and Biomolecular Engineering, Rice University, [2]Departement of Electrical Engineering, Shinshu University

Background

Carbon Nanotubes:
- High specific surface area
- High electrical conductivity
- Ideal material for supercapacitor electrode

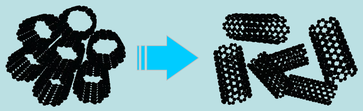

Dispersed nanotubes have a larger surface area to store charge

Supercapacitors:
- Defined by ability to store charge which translates to EVERLASTING battery

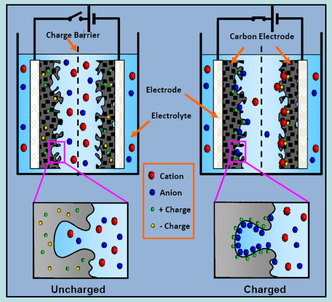

Purpose

Objective: Analyze physical changes during heating of DNA-DWNT films and evaluate its effects during the charge and discharge process

Importance:

ENHANCED ENERGY STORAGE

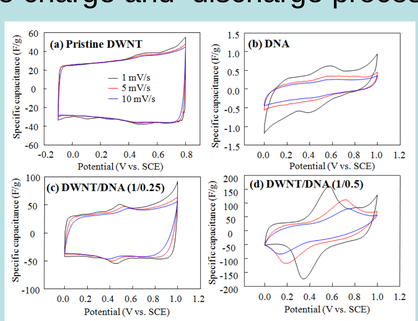

L.Cooper et al. Appl. Phys. Letters **2009** , 95, 233104

Method

Thin Film Fabrication:
- Disperse DWNTs with ssDNA and sonification
- Filtrate into film
- Heat to 600°C

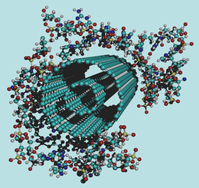

ssDNA wrapped around DWNT

Analysis:
- In-situ Raman
- TEM
- SEM
- TG-DTA
- XPS

TEM

Filtration apparatus

Results

In-Situ Raman:
The outer tube of the heated DNA-dispersed DWNT accepts electrons less readily during the charging process than the non-heated sample

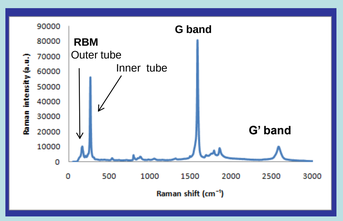

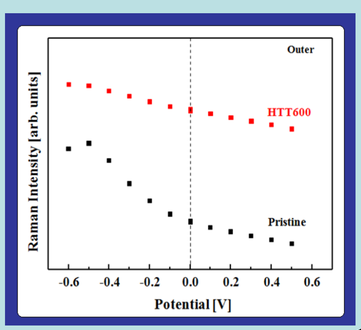

Results…

TG-DTA:
During the heating process, the film decomposes and looses 30% of its weight due to the decomposition of DNA

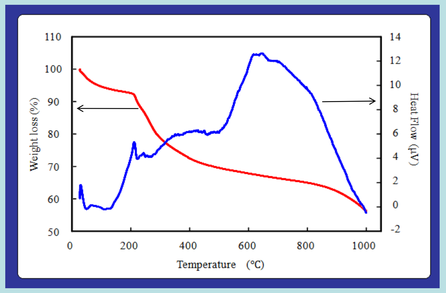

XPS:

Sample I.D.	Na 1s [At.%]	O 1s [At.%]	N 1s [At.%]	C 1s [At.%]	P 2p [At.%]
Pristine	4.928	26.600	7.670	59.050	1.749
HTT600	2.459	8.486	2.586	85.350	1.124

SEM and TEM:
Single stranded DNA disperses DWNT

SEM-DNA/DWNT film

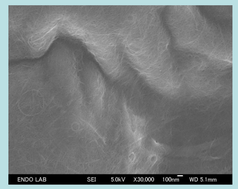

TEM-DNA wrapped around DWNT

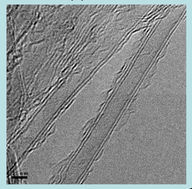

Conclusion

During the heating process, the DNA-dispersed DWNT film decomposes to expose more carbon on the surface leading to a decreased electron acceptance rate during the charge process.

Future Work:
- In-situ Raman at different potentials
- Heat sample to different temperatures
- Look into further applications

The work was supported by the National Science Foundation Grant No. OISE-0530220

http://nanojapan.rice.edu

Acknowledgments

Special thanks to all people at Shinshu University in Endo's laboratory who made the summer internship possible. Also thanks to Sarah Phillips, Dr. Cheryl Matherly , Prof. Junichiro Kono, Prof. Christopher Stanton , and Keiko Packard who made the NanoJapan program such a success.

Temperature Dependent Time-Domain Terahertz Spectroscopy of Pure and Nitrogen-Doped Graphene

Jeffrey Lee,[1] L. Ren,[2,3] J. Kono,[2,3] K. Takeya,[4] R. Kinjo,[4] I. Kawayama,[4] M. Tonouchi,[4] Z. Jin,[3,5] Z. Sun,[3,5] Z. Yan,[3,5] and J. M. Tour[3,5]

1. NanoJapan Program and Department of Mechanical Engineering & Materials Science, Rice University
2. Departments of Electrical and Computer Engineering and Physics and Astronomy, Rice University
3. The Richard E. Smalley Institute for Nanoscale Science and Technology, Rice University
4. Institute of Laser Engineering, Terahertz Photonics Laboratory, Osaka University
5. Department of Chemistry, Rice University

Graphene Background

- Graphene Characteristics:
  - Single layer of carbon atoms
  - Zero-gap semiconductor
  - Exceptional ballistic transport properties
  - High strength
  - High thermal conductivity

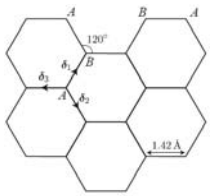

Fig 1: Graphene's hexagonal crystal lattice of carbon atoms

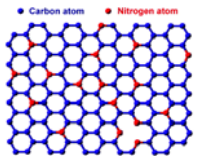

Fig 2: Vacancies and substitutions in the crystal lattice from doping

- Controlled doping is an essential tool in the path to semiconductor applications
  - N-doping: n-type semiconductor
  - B-doping: p-type semiconductor

Purpose

- Observe the low energy carrier dynamics of graphene
  - Understand the effects of doping on the transmittance
  - Understand the effects of temperature on the transmittance
- Explain transmission trends within the Mikhailov theoretical model

Methods

- Terahertz Time-Domain Spectroscopy (THz-TDS) is a method of determining a number of material properties including:
  - refractive index
  - dielectric constant
  - complex conductivity
  - Transmission coefficient
- Production of samples
  - CVD on Copper film
  - N-doped produced by introducing ammonia
  - Transferred to sapphire substrate
- Measurement and Analysis
  - Used THz-TDS to get waveforms
  - Compared substrate and sample
  - Applied FFT to find transmittance

Fig 3: Specimens used in this experiment

Experimental Setup: THz-TDS

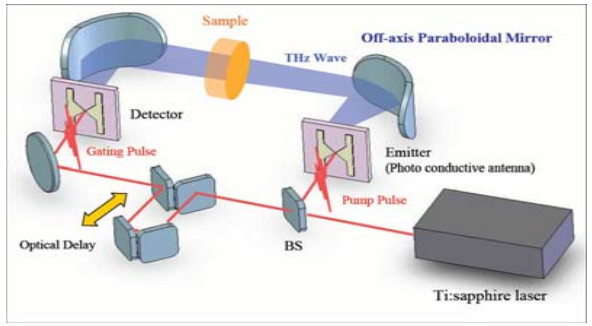

Fig 4: An example room temperature THz-TDS set up

- Two methods of reducing relative humidity
  - Nitrogen purging
  - Vacuum pumping
- Two different emitters
  - Low Temperature grown Gallium Arsenide (LT GaAs)
  - 4-dimethylamino-N-methyl-4-stilbazolium-tosylate (DAST)
- Measurements taken from 10K-300K
  - Used Helium to lower the temperature of the cryostat
- Data averaged over at least 3 readings

Pure and Doped Graphene

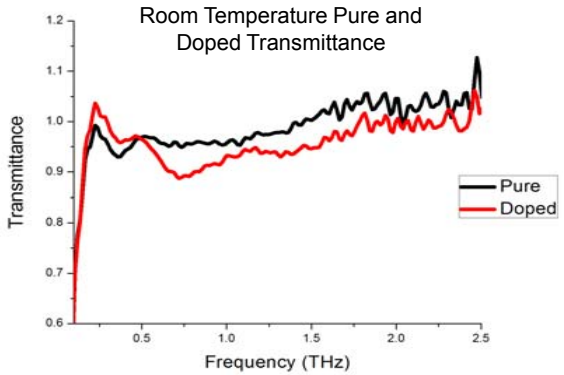

- Pure graphene has a higher transmittance than doped graphene in the range of .5 – 2.5 THz
- Around .7 THz, there is a peak that may be attributed to absorbance
- Both pure and doped have very high transmittance

Temperature Dependence

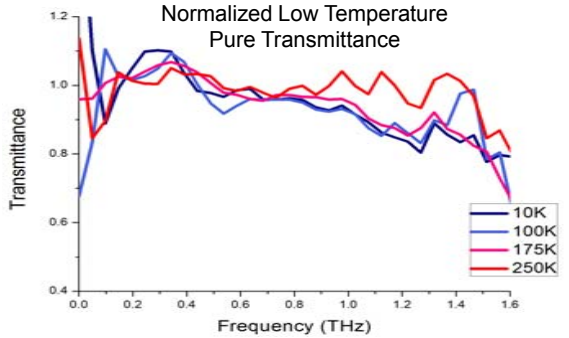

- Positive correlation between temperature and transmittance
- Scattering can be observed in higher energy regions
- Gap suggests a critical temperature between 175K and 250K

Discussion

- Reasons for high transmittance:
  - Both graphene samples had low absorbance or high reflection
  - Different substrate sample thicknesses
- Doping and Temperature Effects
  - Doping increases intraband absorbance
  - Temperature broadens the zero-frequency peak of the intraband conductivity

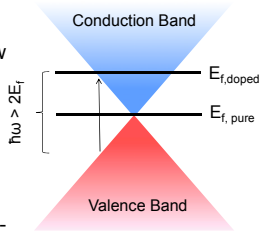

Fig 5: Doping Effects on Fermi Energy due to carrier densities

Conclusions

- Monolayer graphene has either a low absorbance or high reflection
- Doping is observed to decrease transmittance
- Increasing temperature is observed to increase transmittance

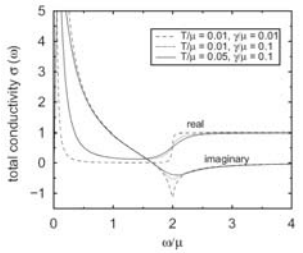

Fig 6: Conductivity according to the Mikhailov theoretical model

Sources:
Fig 2: Dacheng Wei, *Nano Letters* **2009** *9* (5), 1752-1758
Fig 4: http://www.riken.jp/lab-www/THz-img/English/annual_gas.htm
Fig 6: S. A. Mikhailov, Microelectronics Journal 40, 712 (2009)

This material is based upon work supported by the National Science Foundation under Grant No. OISE-0530220.

Integration of ZnO Nanorod Biosensor with Field-Effect Transistor

Marcus Najera[1,2], Ken-ichi Ogata[2], Hideaki Dobashi[2], and Shigehiko Sasa[2]
NanoJapan Program[1], Rice University and Department of Nanotechnology,
North West Vista College
Nanomaterials Microdevices Research Center, Osaka Institute of Technology[2]

I. Purpose

Recent technological advances in fabrication of novel hybridized semiconductors, and inorganic nanomaterials may provide the tools necessary to immobilize bio-molecules such as enzyme substrates. The objective of this research is to combine extended-gate field-effect transistors (EG-FETs) with biosensing devices utilizing high aspect ratios of ZnO nanorods (NRs) to achieve a high surface area for glucose immobilization. EG-FETs provide a useful mechanism by aiding in sensitivity, and utilizing energy more efficiently. Diabetes mellitus is a chronic disease which has proven difficult to cure. As of now the best route is precise measurements to manage in keeping blood sugar levels within standard deviation. With diabetes on the rise it is important to develop modern techniques to aid as much as possible.

II. Methods

1)Electron-Beam Deposition

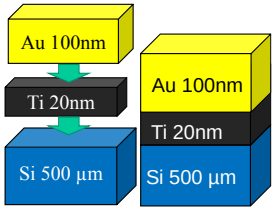

- The base substrate used in probing of glucose detection is Si(004)
- Si is prepared via cleaving with diamond pen, and organic cleaning
- By means of electron-beam deposition titanium is deposited in a 20nm layer, followed by gold deposition of 100 nm

The Silicon substrate candidacy is based on positive results from prior research at the *Nanomaterials Microdevices Research Center at the Osaka Institute of Technology*. Titanium is added to the silicon substrate as a cost effective diffusion barrier as well as an adhesive for gold to substrate deposition. It should be noted that prior research has shown gold to be an optimal layer for ZnO NRs to be grown on

2) ZnO Nanorod Growth

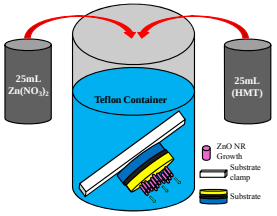

- (10mM), (30mM), (100mM) 25ml ZnNT solutions prepared
- (10mM), (30mM), (100mM) 25ml Hexamethylenetetramine solutions prepared
- Substrates are fixed via clamp
- Solutions are mixed into Teflon 5 containers
- Substrate is placed as seen in the figure in a nylon container
- Teflon container undergoes microwave radiation for 3hr at 95ºC

Zinc Nitrate HMT

$Zn(NO_3)_2 \times 6H_2O + C_6N_4H_{12} \rightarrow ZnO + H_2O + 2OH^-$

ZnO NRs have a high aspect ratio which allows optimal immobilization due to a high surface area to volume ratio. The demonstrated ZnO low temperature growth of NRs is a very promising method for integration of biosensors. Previously low temperature, selective growth has been demonstrated.

3)Fabrication of Biosensor

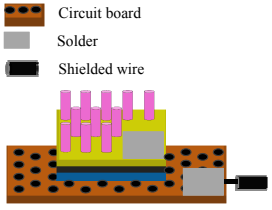

- Addition of epoxy to the backside of circuit board and solder shielded wire
- Substrate fixed on circuit board with double sided sticky tape, and conductive silver paste added from solder to gold substrate
- Add epoxy everywhere except the top of substrate to prevent exposure to aqueous solutions

Biosensor fabrication steps stated are to ensure the substrate is in a fixed position, has a connection for parameter analysis, and has a shield against exposure. The solder selected for this experiment was 60% tin 40% lead. Epoxy was a standard commercial hydrophobic material.

4)Immobilization of Glucose Enzyme

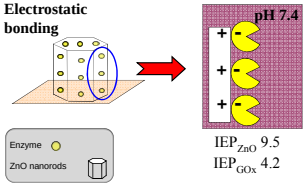

- 15 min for glucose immobilization
- Provides a very quick method
- Less immobilization compared to covalent method
- Bonds are weak compared to covalent method

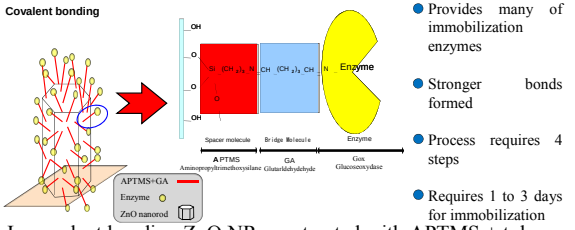

- Provides many of immobilization enzymes
- Stronger bonds formed
- Process requires 4 steps
- Requires 1 to 3 days for immobilization

In covalent bonding ZnO NRs are treated with APTMS + toluene aqueous solution. Next the substrate is then transferred to a GA aqueous solution. To complete the covalent bonding process one drop of GOx is applied on the substrate and left for 3 days. In the case of electrostatic bonding one drop of glucose oxidase is applied on the substrate for 15 min. After immobilization a colormetric method was used to check enzyme activity.

4)Integration of Extended- Gate Field-Effect Transistor

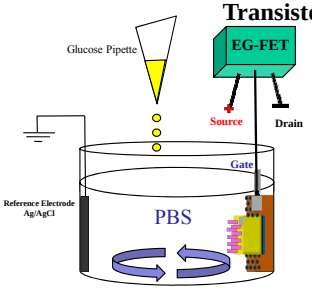

- Biosensor is submerged in solution
- EG-FET is connected to shielded wire
- Electrical baseline is acquired
- Glucose is added and effects in source and drain are measured

III. Results

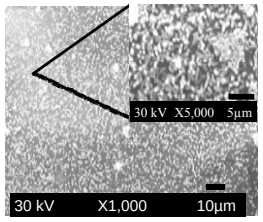

SEM images of ZnO NRs peak on Au/Ti/Si(004) substrate display successful growth in the (0002) axis. The displayed NRs have a average diameter of 400 nm.

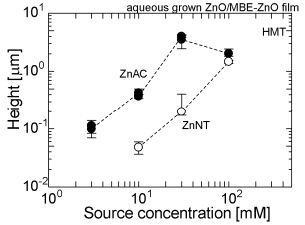

The alpha-step characterization provides a correlation between concentration of precursors and height of NRs. In our parametric trials 100mM equimolar solutions appear to be the best choice.

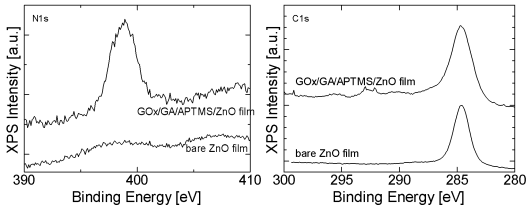

X-ray photoelectron spectroscopy (XPS) spectra of ZnO NRs/AU/Ti/Si(004) indicate that enzymes have been successfully immobilized. The XPS spectra of N1s, C1s indicates the presence of more nitrogen and carbon in treated substrates with immobilized glucose oxidase.

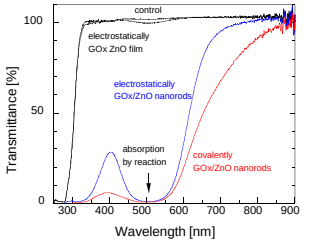

- Shows difference in immobilization from ZnO film vs NR's surfaces
- Shows difference in electrostatic and covalent bonds
- NRs peak is saturated indicating that more immobilization has taken place

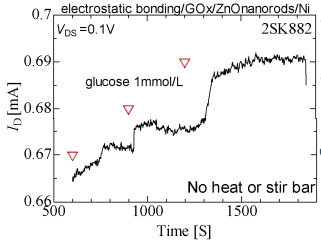

- Glucose sensing is demonstrated
- A relationship exists between current and addition of glucose
- Under 0.1mM of glucose can be detected with optimization

IV. Conclusions

Low temperature growth of ZnO NRs and integration of EG-FET on Au/Ti/Si(004) substrate was conducted. GOx was immobilized on the high surface area of ZnO NRs and has been characterized by SEM, XPS, and colorimetric measurements. EG-FET will increase current as a result lower quantities of glucose can be detected. Future integration of FET substrate with selectively grown ZnO NRs is next to be investigated.

This research was supported by the National Science Foundation Grant No. OISE - 0530220

Spatially-Resolved Electroluminescence of Individual Au Nanoparticles

Nicholas S Riggall 1, 2, Chi Chen 2, Norihiko Hayazawa 2, Satoshi Kawata 2
1. NanoJapan Program, Rice University and Department of Nanotechnology
2. Nanophotonics Laboratory, RIKEN National Laboratory

BACKGROUND

STM-EL: Scanning Tunneling Microscope Electroluminescence
Is a novel method of examining the electroluminescent properties of materials with extreme precision. This technique allows for topographic and EL analysis of materials.

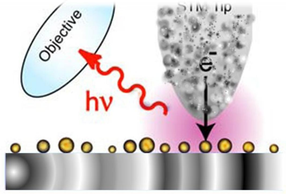

Scheme of STM-EL

STM-EL uses STM's extreme spatial resolution to permit resolute EL probing of conductive materials. In this project gold nanoparticles are examined using STM-EL to try and determine EL properties and prove abilities of STM-EL.

Photoluminescence techniques have increased far beyond current electroluminescence techniques, yet knowledge of materials' electroluminescent properties is integral to improving technologies such as LED and solar cells.

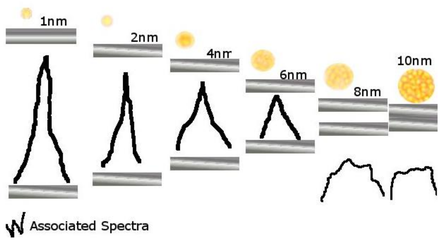

This shows the expected transition sizes as particles begin to exhibit plasmon resonance, and a broader spectra of emission.

Smaller particles have larger band gaps and individual peaks corresponding.

Using STM-EL we hope to determine this transition point.

MATERIALS AND METHODS

Via STM-EL Gold Nanoparticles were analyzed on a flat, conductive, freshly cleaved graphite surface.

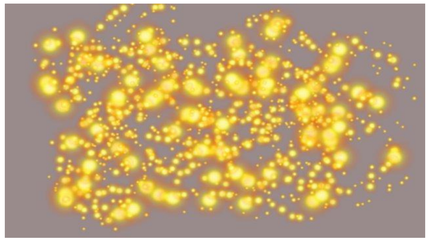

1. Optimal particle distribution was achieved by leaving colloid solution on for 75 seconds.
2. Sample was then dried using Nitrogen gas at low pressure.
3. Particle size and distribution confirmed via Atomic Force Microscopy

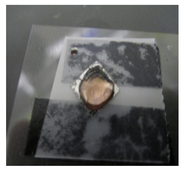

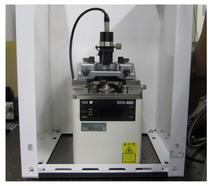

MATERIALS AND METHODS

Particle size and distribution on surface is viewed via Atomic Force Microscope.

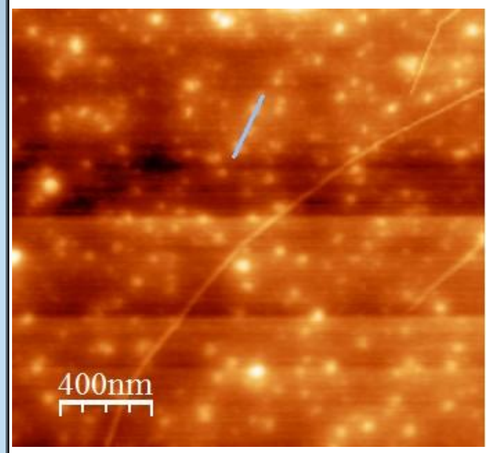

Size (nm) corresponding to particles crossed by line in picture of AFM scan.

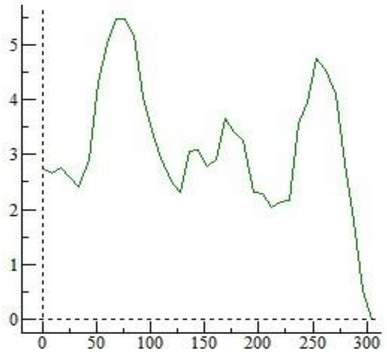

The sample can then be analyzed in the STM-EL. When an isolated particle is found, it can be pinpointed and targeted by the STM-EL probe and stimulated with a varying bias until the emission is observed. At some point between 5 and 10nm it is expected that the band gap will be too small to be observed and instead a broad spectrum indicative of Plasmon Resonance will be observed.

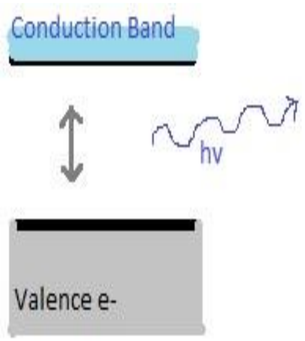

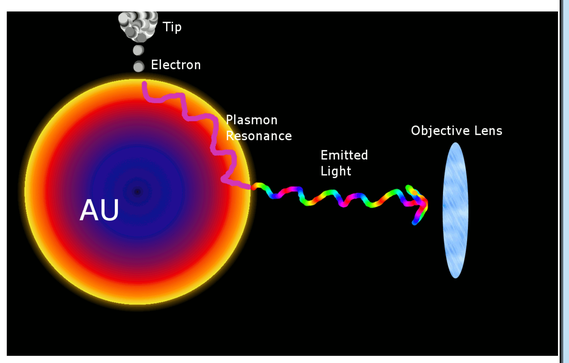

When these Electroluminescent properties are determined in the STM-El it will allow for the surface to be characterized in terms of both the topography and the respective light wavelengths emitted.

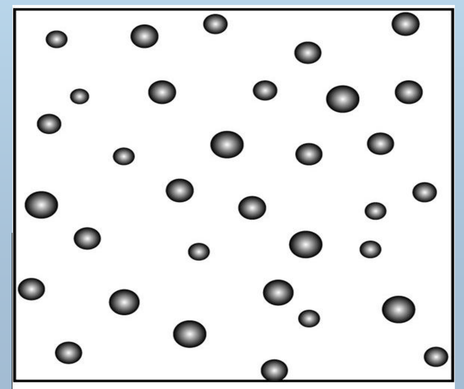
Topographic Image

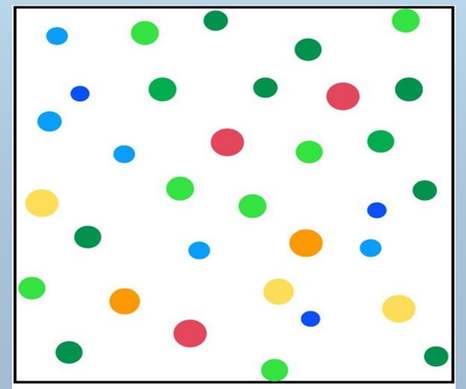
EL Photon Image

RESULTS

This experiment involved extensive characterization of gold nanoparticles in the target range. The y were placed and studied upon both Mica and Graphite surfaces via Atomic Force Microscopy. The difficulties associated with attaching completely bare particles to a bare, flat surface led to a difficult characterization process. The deposited particles' distribution was unpredictable and difficult to control and it was difficult to prevent particle clumping. More experimentation should be done to find more efficient techniques for bare particle to bare surface attachment.

During the STM-EL analysis it also became apparent that the bias of the tip and sample can cause the unattached particles to drift or be pushed by the probe and thereby be difficult to isolate and scan. The STM-EL is still capable of this analysis though better ways must be found to attach and isolate the particles without compromising the structure, conductivity, or particle surface.

CONCLUSIONS

As Electroluminescent properties continue to be integral to the development of technologies including solar cells and LED it is important that this research be continued. As the problem for particle drift is addressed we will hopefully be able to analyze individual particles and learn more about the properties of nanomaterials. Currently PL technology is far more capable, but with the development of this STM-EL technique the gap will be closed. With STM-EL's ability to analyze materials on the angstrom scale we can hopefully greatly assist the fields of nanotechnology and improve technology such as LED and solar cells.

FUTURE WORK

In the future the project the project will be continued to pursue mapping of the quantum properties of gold nanoparticles <10nm. Different ways of isolating the nanoparticles for probing as well as different methods of distribution will be explored.

STM-EL is a difficult procedure in some ways, and hopefully via further use, the process will become more streamlined and easier to apply to new scenarios.

BIBLIOGRAPHY

"I. Horcas, R. Fernandez, J.M. Gomez-Rodriguez, J. Colchero, J. Gomez-Herrero, and A.M. Baro, Review of Scientific Instruments 78, 013705 (2007)".

Chi Chen *et al. Science* 325, 981 (2009)

N. Nilus *et al. Phys. Rev. Lett.* 84, 3994 (2000)

F. Silly *et al. App. Phys. Lett.* 79, 4013 (2001)

http://www3.interscience.wiley.com/cgi-bin/summary/112606367/SUMMARY

http://www.springerlink.com/content/x2j17w3183777551/

ACKNOWLEDGMENTS

This research was supported by the National Science Foundation Grant No. OISE-0530220

Electron Spin Resonance of Graphite and Graphene

C. Sewell,[1] A. Mahjoub,[2] A. Takuto,[2] and Y. Ochiai[3]
[1]NanoJapan Program, Rice University, Houston, Texas and Department of Physics and Engineering Physics, University of Tulsa, Oklahoma
[2]Department of Nanomaterial Science, Chiba University, Chiba, Japan

Introduction

Gaphene-

❖Zero effective mass of electrons due band structure
- ➢ Causes high electron mobility (100 times that of silicon at room temp)

❖Small spin-orbit coupling of carbon atoms
- ➢Highly desirable in spintronic devices

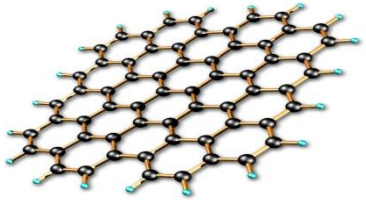

Graphene band structure

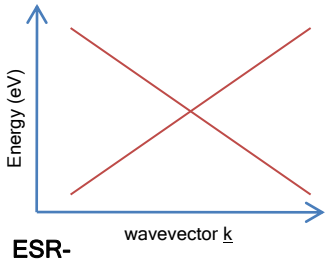

ESR-

❖Used to explore spin properties of electrons in graphite and graphene
❖Will determine g-factor using this method

Methods and Sample Prep

❖Sample subjected to constant 9.2 GHz microwave frequency ν
❖DC magnetic field B_0 scans over sample
❖When B_0 satisfies $\hbar\nu = g\mu_B B_0$ electrons absorb microwave photon energy
❖Lock-in amplifier separates signal from noise
❖Produces absorption peaks as function of magnetic field strength

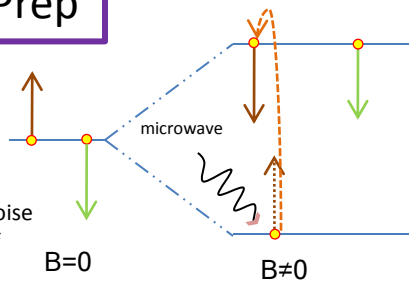

❖Used kish and HOPG graphite
❖Prepared sample using exfoliation and scraping techniques
❖Light pink areas in right photo are graphene
❖Glue and green areas are graphite

Optical Microscope 100X magnification

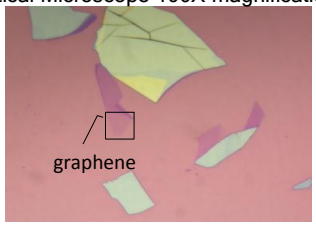

Results

Graphene

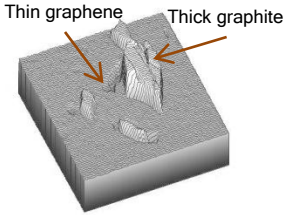

❖Field based ESR insufficiently sensitive to detect the microwave absorption of graphene
- ➢Size of sample produced by exfoliation is to small
- ➢Interference from surrounding graphite dwarfed the graphene absorption

Graphite Power Dependence-

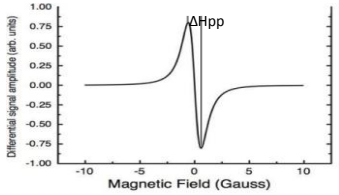

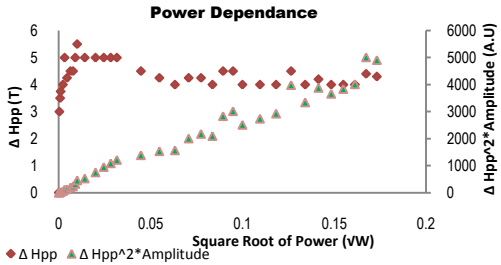

T_1	$2.35*10^{-12}$ s
T_2	$8.6*10^{-9}$ s
g-factor	2.0034

Conclusion

❖Detected graphite absorption spectrum
❖Derived graphite g-factor
❖Calculated T_1 and T_2 relaxation times

❖Will implement low temperature aspect to power dependant testing
❖Must use resistive techniques in order to determine graphene g-factor

This material is based upon work supported by the National Science Foundation under Grant No. OISE-0530220.

http://nanojapan.rice.edu

Absolute Quantum Tunneling Rate Measurements in NanoMagnets

Aleksandra Simicevic[1], Shunsuke Yoshii[2], Go Tanaka[2], Misaki Hayashi[2], Takaharu Tashiro[2], and Hiroyuki Nojiri[2]

[1]NanoJapan Program, Rice University, USA and Department of Civil and Environmental Engineering, Louisiana State University, USA

[2]Institute for Materials Research, Tohoku University, Japan

INTRODUCTION

High spin single molecule magnets

- Applications:
  - Nanoscale magnetic memory
  - Quantum computing
- Features
  - Distinct magnetization states
  - Store memory in “spin up” or “spin down” states

What is Quantum Tunneling of Magnetization (QTM)?

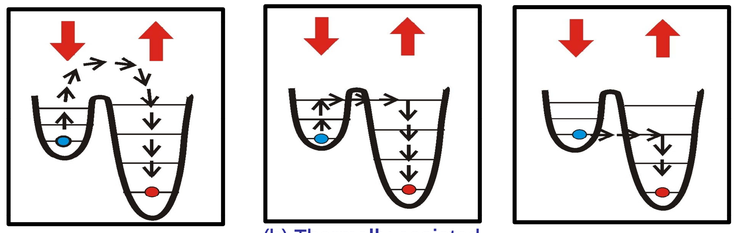

(a) Thermal relaxation (b) Thermally assisted tunneling (c) Quantum tunneling

- Configurations of particles described by quantum numbers. Spin quantum number defines value and orientation of spin.
- Zeeman energy level is degenerate at zero magnetic field.
- Applied magnetic field alters energy and breaks degeneration.

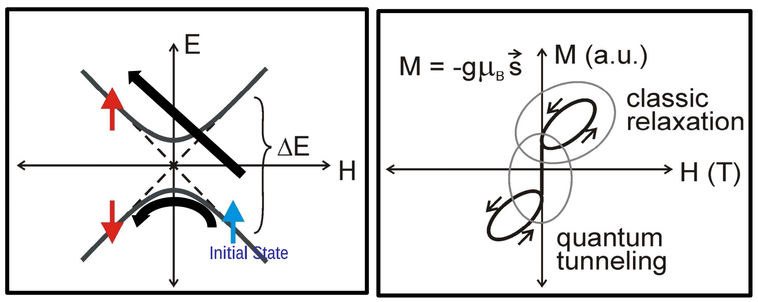

Zeeman graph shows the splitting of an energy level as a magnetic field is applied.

- *Classic physics:* An electron’s different orientations are permanently separated and are assumed to remain in the same orientation.
- *Quantum physics:* In a region, occurring around a zero magnetic field, electron may switch orientations and tunnel through the energy barrier into a different energy state. This transition is called *quantum tunneling*.

OBJECTIVE

- To determine the origin of absolute spin reversals in single molecular magnets in a two-level spin system of Cu^{2+} ions doped in a $Ca(PO_3)_2$ glass
- Use steady magnetic field and pulse field combination to find absolute reversal rate
- Variables:
  - Temperature (0.4 K -1.5 K)
  - Sweep rate (2000 T/s - 6000 T/s)
  - Density of ions (1% - 4%)

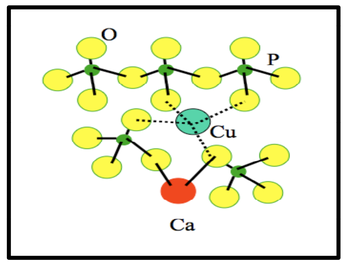

METHOD

Magnetization measurements under pulsed magnetic fields

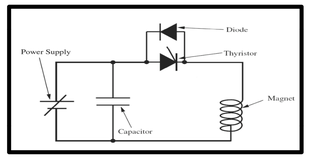

Generator of pulse fields

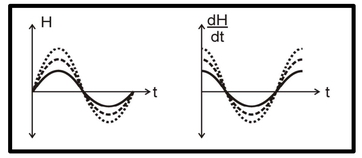

Magnetic field and sweep rate

Schematic of magnetization measurements under pulsed magnetic fields

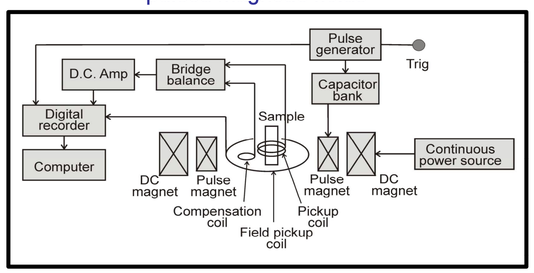

- Steps:
  - Sample concentration preparation
  - Cooling system (temperature variable cryostat with He system)
  - Signal detection (standard induction method with pick-up coils)
  - Pulsed field + steady field (to control the initial spin state) measurements

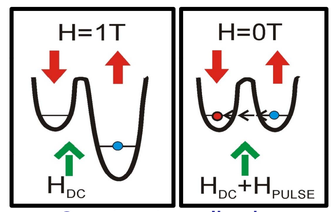

Quantum tunneling in two-level system under pulse and steady fields

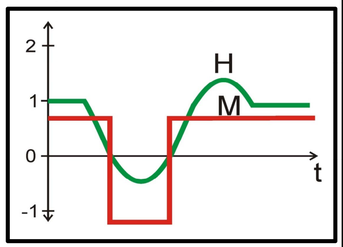

RESULTS

- Quantum tunneling found:
  - Rapid change in magnetization with zero magnetic field

Magnetization vs. magnetic field

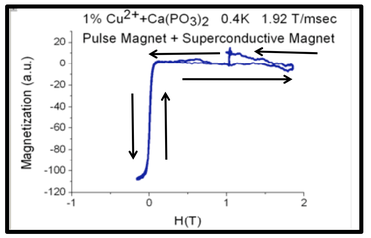

Pulse magnet + Superconductive magnet

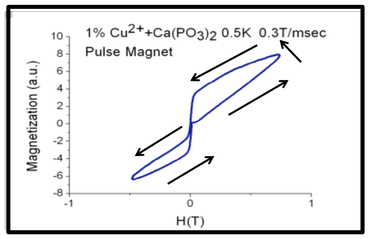

Pulse magnet

- Quenched relaxation:
  - Little hysteresis
  - Little dependency on temperature change
- Tunneling gap is 25 mk
- Large reversal rate (close to 1) occurs at 400 mK

Absolute reversal rate

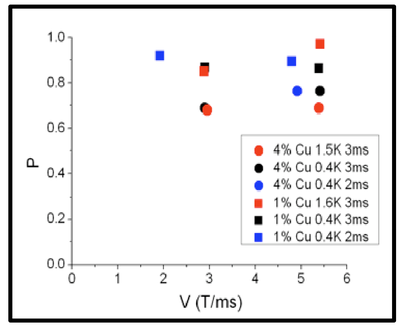

CONCLUSIONS

- In quantum tunneling-region, quantum tunneling occurs even though temperature is larger than ten times the tunneling gap
- Quantum tunneling produced by fast-sweeping fields may be possible at higher temperatures

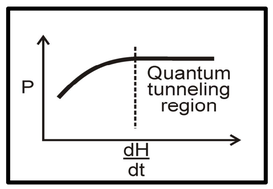

Reversal rate vs. sweep rates

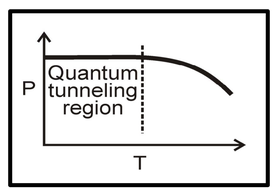

Reversal rate vs. temperature effects

ACKNOWLEDGEMENTS

Research conducted at the Institute for Materials Research in Tohoku University, Sendai, Japan

This material is based upon work supported by the National Science Foundation under Grant No. OISE-0530220

Characterization of Phosphorus Deposition onto Silicon (111) 7x7 Nanostructures for Applications in Quantum Computing

Kirby Smithe[1,2], Tomoya Arai[2], Ryo Tomita[2], Kohei M. Itoh[2]

1. NanoJapan Program, Rice University and Department of Physics and Engineering Physics, University of Tulsa
2. Department of Applied Physics and Physico-Informatics, Keio University

Purpose

All-Silicon Quantum Computer[1]

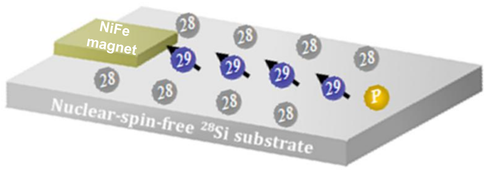

^{28}Si — ^{28}Si used as a substrate because it is spin-free.

^{29}Si — ^{29}Si used as quantum bits, nuclear spins acting as Boolean logical data.

^{31}P — ^{31}P used for initialization, readout, and maintaining an external magnetic field.

NiFe magnet used to generate the external magnetic field of ~7T.

Benefits of an All-Silicon Quantum Computer

- Quantum superposition allows for parallel processing on a single wire of qubits.
- Techniques for developing silicon already exist.
- Silicon can be scaled to larger devices.

Classical *n*-bit Architecture

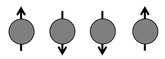

Classically, a byte with n bits can represent one of 2^n numbers. Operations must be done one at a time.

Quantum *n*-bit Architecture

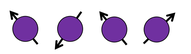

Quantum mechanics allows for one byte to be in a superposition of all 2^n number states. 2^n operations can be done simultaneously.

Experimental Methods

3. Molecular Beam Epitaxy

Slow cooling to room temperature eliminates small defects. 0.014 L doses of ^{31}P are evaporated and adsorbed onto the ^{28}Si step edges at various temperatures.

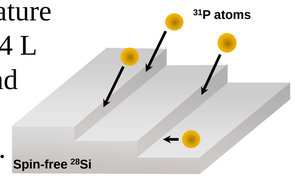

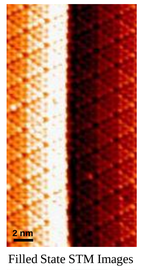

Filled State STM Images

4. Scanning Tunneling Microscopy

Surface structure of substrate and deposited atoms are observed with the STM. The number of deposited ^{31}P atoms is counted and graphed as a function of temperature.

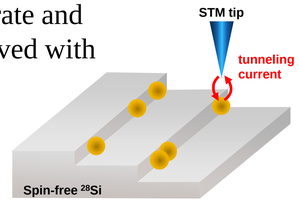

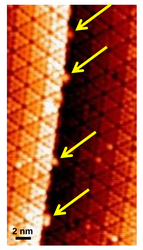

Results and Conclusions

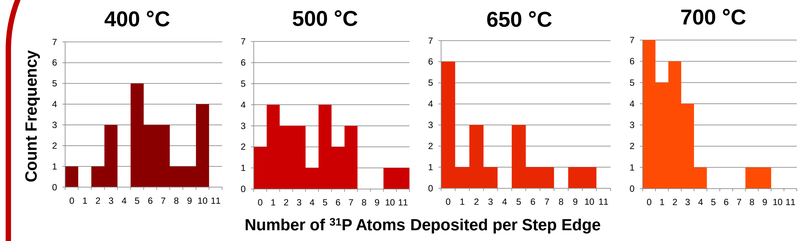

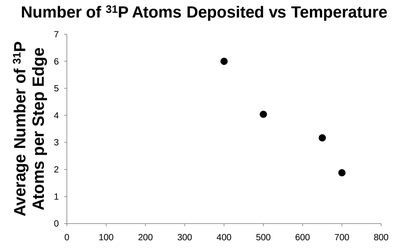

The deposition rate of ^{31}P does have a temperature dependence in that more ^{31}P atoms are deposited along the ^{28}Si step edges at lower temperatures. At higher temperatures, the ^{31}P atoms have higher thermal energy, which inhibits deposition.

Discussion

The results for ^{31}P deposition at 400 °C are the most significant, as the ^{29}Si nanowires are grown at this temperature. The willingness of ^{31}P atoms to adsorb onto the ^{28}Si step edges at 400 °C indicates that fabricating the desired ^{29}Si and ^{31}P nanowires is possible and will be a rather straightforward process.

Experimental Methods

1. Mechanical and Chemical Polishing

Ultrafine polishing at a 1° angle in the [111] direction and a 3° tilt in the azimuthal direction produces step edges with kinks.

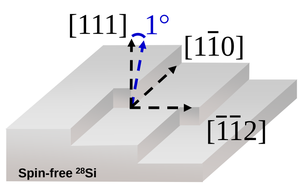

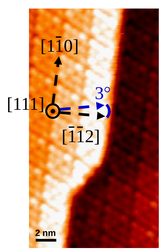

Filled State STM Images

2. Long Duration DC Annealing

Rapid flash heating to 1300°C cleans the substrate. 10 hours of 1.4 A annealing at 800° C in the kink-up direction straightens the edges via electromigration.

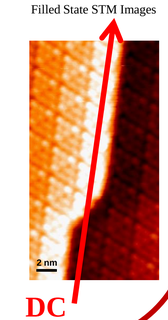

Results

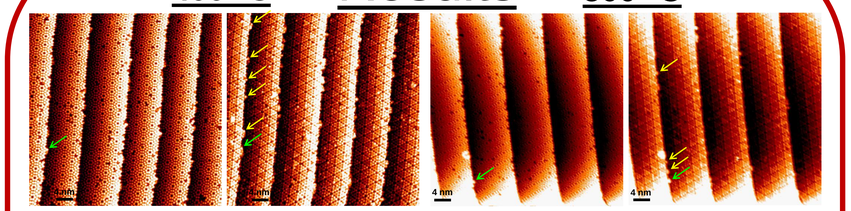

Empty State STM Image | Filled State STM Image | Empty State STM Image | Filled State STM Image

Green arrows indicate atoms that are not ^{31}P.

Phosphorus is visible only in the filled state images!

Yellow arrows indicate atoms that might be ^{31}P.

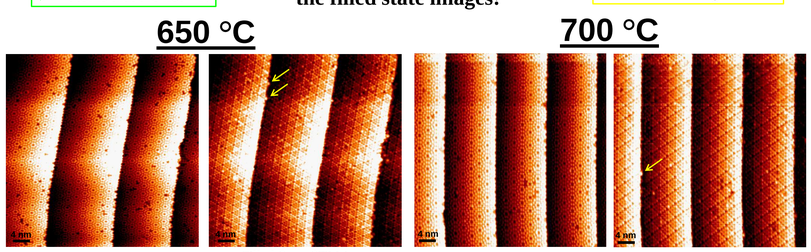

Empty State STM Image | Filled State STM Image | Empty State STM Image | Filled State STM Image

The numbers of ^{31}P atoms per step edge is tallied and displayed in histograms. The results are then averaged and graphed as a function of temperature.

Future Work

- Scanning tunneling spectroscopy of deposited ^{31}P atoms
- Annealing time, deposition time, and azimuthal angle dependence of ^{31}P deposition
- Deposit ^{29}Si nanowires with ^{31}P at the ends

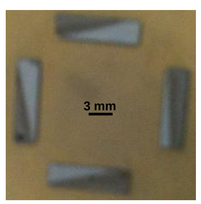

3°, 7°, 11°, 15° azimuthal angle substrates

References

[1] Kohei M. Itoh, Solid State Communications **133**, 747. (2005).

This material is based upon work supported by the National Science Foundation under Grant No. OISE-0530220.

Additional thanks are due to Professor Junichiro Kono, Professor Christopher Stanton, Dr. Cheryl Matherly, Sarah Phillips, and Keiko Packard for their contributions to the NanoJapan Program. Some objects and images are courtesy of Tomoya Arai.

http://nanojapan.rice.edu

Single Crystal Growth of Diamond And Its Optical Characterization

Norman Wen[1,2,3], Yusuke Okura[3], Makoto Kuwano[3], Go Yusa[3]

1. *NanoJapan Program, Rice University*
2. *Department of Mechanical Engineering & Department of Materials Science and Engineering, University of California, Berkeley*
3. *Department of Physics, Tohoku University, Japan*

Motivation

Quantum Computing

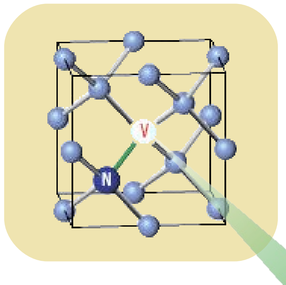

Nitrogen impurities form point defects in diamond crystal lattice

Nitrogen Vacancy center serves as a stable **qubit** at room temperature

Unpaired Electron spins can be manipulated with magnetic stimuli and detected optically

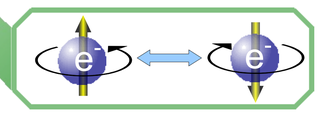

Goal: Single crystal diamond with high growth rate

Methods

Diamond Substrate Preparation

1. Evaporate Titanium Mask

Photolithography is used to pattern and evaporate Ti on to substrate for **selective growth**

Under selective growth, the **growth rate** can be determined

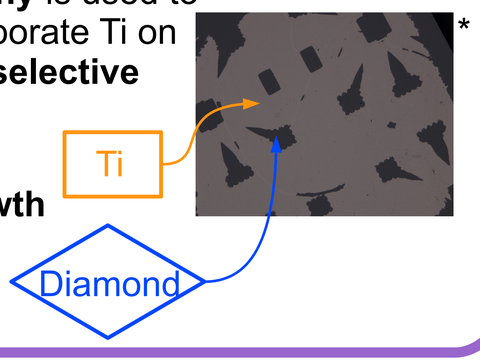

*

Methods cont.

2. Chemical Cleaning

Substrate is cleaned to remove contaminant particles by ultrasonic cavitation

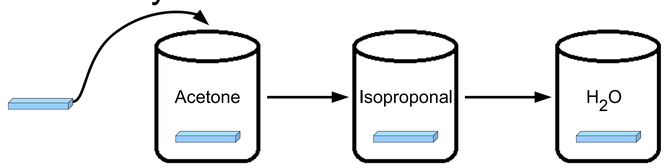

3. Hydrogen Etching

Substrate is exposed to hydrogen plasma to etch non-diamond species

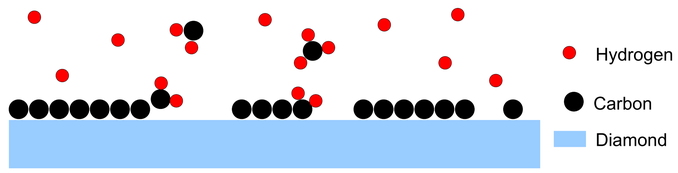

Diamond Growth

4. Chemical Vapor Deposition

Methane gas is used as a carbon source for diamond growth

Parameters:

- Temperature
- Pressure
- CH_4 concentration

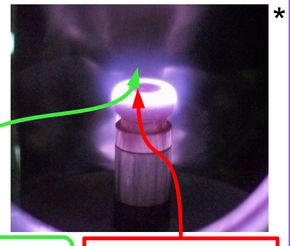

*

Results

Polycrystal Density

Determined using images taken using an optical microscope with a Nomarski filter

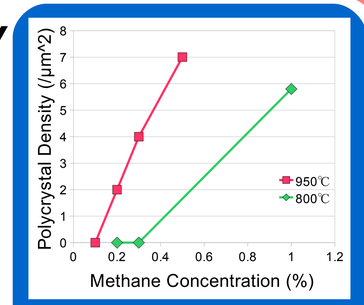

Growth Rate

Determined by surface profiler before and after growth

Surface Profiler

*

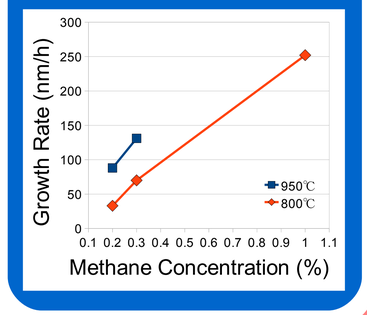

Conclusions

Single crystal diamond was successfully grown homoepitaxially with thickness up to 1 μm

Growth rate increases with higher temperature and methane concentration

Polycrystal formation is directly related to contaminant particles, making substrate preparation important, and increases with higher temperature and methane concentration

FUTURE WORK

Characterization using cathode luminescence, Raman spectroscopy, and photoluminescence

Research conducted at Tohoku University as a participant in the Rice University NanoJapan 2010 Program sponsored by the NSF-PIRE grant.

Sincere thanks to Professor J. Kono, Professor C. Matherly, and Sarah Phillips for making the NanoJapan program possible. *Images courtesy of the Quanta and Information Group, Tohoku University

References

1. David D. Awschalom *et. al*, "The Diamond Age of Spintronics", Scientific American, **297 (**2007)